Energy 238 (2022) 121815

Contents lists available at ScienceDirect

Energy

journal homepage: www.elsevier.com/locate/energy

Preliminary investigation of the influence of equations of state on the performance of $CO_2 + C_6F_6$ as innovative working fluid in transcritical cycles

G. Di Marcoberardino [a, *], E. Morosini [b], G. Manzolini [b]

[a] Università Degli Studi di Brescia, Dipartimento di Ingegneria Meccanica Ed Industriale, Via Branze, 38, 25123, Brescia, Italy
[b] Politecnico di Milano, Dipartimento di Energia, Via Lambruschini 4, 20156, Milano, Italy

ARTICLE INFO

Article history:
Received 21 September 2020
Received in revised form
28 July 2021
Accepted 13 August 2021
Available online 17 August 2021

Keywords:
CO_2-Blends
Equation of state
Hexafluorobenzene
Thermodynamic assessment

ABSTRACT

sCO_2 power cycle is the most investigated and most promising technology for replacing conventional steam cycle in CSP plants. Nevertheless, the efficiency of sCO_2 power cycle is strongly penalized by high ambient temperatures which are typical of favourable CSP locations. This paper focuses on a new working fluid for power cycles which consists of CO_2 blended with C_6F_6. The addition of C_6F_6 increases the fluid critical temperature allowing for a condensing cycle for ambient temperatures up to 45 °C. The calculated gross mechanical efficiency of the innovative cycle is around 42% when adopting a typical Peng Robinson equation of state with van der Waals mixing rules for a maximum operating temperature of 550 °C and a minimum cycle temperature of 51 °C. This performance varies just of ±0.1% if the prediction of the binary interaction parameter of the Peng Robinson is over- or under-estimated by 50%, but more significantly if other equations of states are adopted (up to 1% points). Moreover, a detailed analysis on the operating conditions of the cycle components highlighted that components design is affected by the adopted EoS. A sensitivity analysis is then performed to identify where the largest differences in predicting the efficiency of the cycle occur.

1. Introduction

Power generation from high temperature concentrating solar power (CSP) plants is a promising technology [1], although it is still characterized by significant capital cost and a resulting Levelized Cost of Electricity (LCOE) higher than competitive renewable and fossil fuel technologies [2]. Typical power plants applied to CSP are based on traditional steam cycle that can achieve a gross mechanical efficiency in the range of 38%–42% [3–5], depending on the cold sink temperature, with some techno-economic disadvantages (high capital cost, large turbomachinery). The typical CAPEX for this CSP concept is around 6000–4000 $/kW, with LCOE that can strongly varies from 110 to 270 $/MWh, mainly depending on the financial costs of the investments [2]. Today, the maximum temperature of CSP plants is given by the steam cycle technology and the adopted Heat Transfer Fluid (HTF): in commercial solar tower power plants, a maximum temperatures of 565 °C can be reached with molten salts (typically Solar Salts which is a binary nitrate eutectic 60%$NaNO_3$/40%KNO [6]) while, in emerging plants this limit can be increased up to 700–750 °C using liquid sodium [3,7]. Recently, many efforts have been spent towards innovative cycles trying to overcome some of the steam Rankine disadvantages. Supercritical CO_2 (sCO_2) cycles is certainly one of the most promising solution with several demonstration concepts worldwide [8]. sCO_2 cycles are characterized by extremely compact machinery and simple layouts: no bleedings, no steam drums, and a minimum operating pressure above the atmospheric pressure are the main advantages of sCO2 cycles over its traditional alternative [9]. Over the last years, many studies focused on pure sCO_2 cycles starting from simple recuperative cycle configuration and exploring new and alternative configurations [7,10–12]. At the current state of the art, the sCO_2 recompressed cycle can reach efficiencies up to 41.8%, at $T_{max} = 550$ °C, and up to 48.9% at $T_{max} = 700$ °C [4]. Most of the efforts in the scientific literature is related to the reduction of the compressor power consumption that strongly affects the cycle efficiency. This becomes crucial when no low temperature coolant (i.e. cold water below 20 °C) is available for the power cycle such as in the typical hot and arid environment for CSP applications. As the

* Corresponding author.
E-mail address: gioele.dimarcoberardino@unibs.it (G. Di Marcoberardino).

https://doi.org/10.1016/j.energy.2021.121815

lower the temperature at the inlet of the compressor (minimum cycle temperature) the better is for the cycle efficiency, the resulting minimum pressure of sCO_2 cycles is usually near the critical point [13], presenting some difficulties in the design of the compressor [14].

An innovative solution investigated within the H2020 European project SCARABEUS [15] is the transcritical cycle where the gas compression phase is replaced with a liquid compression, hence substituting the compressor with a pump. A working fluid for these applications should have a critical temperature above 70 °C, and a relatively low critical pressure to exploit higher compression ratios, while keeping the same advantages of pure CO_2 over steam Rankine cycle, as the cycle compactness. Binary CO_2-based mixtures can be adopted to overcome this hurdle [16]: blending CO_2 with another fluid, with a higher critical temperature, can increase the critical temperature of the resulting mixture with respect to pure CO_2, thus ensuring liquid phase conditions at the inlet of the compression phase for typical CSP application with a minimum cycle temperature around 50 °C.

Moreover, the thermo-physical properties of the dopant in the CO_2 based mixture have an impact on the low-pressure side of the cycle. Indeed, the pumping step is characterised by two opposite effects: on one hand, the higher the temperature at the outlet of the pump, the closer the working fluid is to the maximum cycle temperature, thus reducing the required thermal power input of the cycle; on the other hand, a high temperature increase in the compression step negatively affects the power consumption, due to the higher compressibility effects in the pump. In addition, the pump consumption is directly proportional to the specific volume of the fluid, so the higher the mixture density the lower is its pumping power. Similarly, the heavier the molecular mass of the working fluid and the higher its complexity, the lower is the expansion work. As an example, Table 1 shows the pump (or compressor) power consumption of three different cycles with respect to the power produced by the turbine, for various working fluids that can be adopted in CSP application: (i) steam, (ii) pure CO_2 and (iii) a CO_2-based mixture (CO_2 + Propane, with $z_{CO2} = 30\%$). While for the steam Rankine cycle, the pump consumption is very limited (3% of the turbine power), in the sCO_2 cycles the compression power is significant (more than ten times higher than the steam cycle): this significant difference is due to the different physical state at which the compression occurs in the two cases. In addition, this difference is present in the temperature rise across the compression step with a direct consequence of the compressibility effects along the pumping process. On the other hand, the CO_2-based mixtures can still achieve a subcritical pumping step like steam Rankine cycles, but much closer to the critical point of the working fluid, and therefore having a compression consumption in between the one of the Rankine and the sCO_2.

Previous works on CO_2 mixtures for power cycle identified some potential candidates as organic compounds, noble gases or inorganic compounds, depending on different heat source applications. If organic compounds, such as hydrocarbons or refrigerants, are selected as blending components, the limiting factor becomes the thermal stability of the compounds themselves. Nevertheless, the transcritical cycle with organic compounds blending CO_2 could outperform pure sCO_2 cycle in terms of net electric efficiency when considering heat sources with medium temperatures such as geothermal and biomass plants or waste heat recovery applications (around 350–450 °C), [17–21]. The benefits of CO_2 blended with hydrocarbons in a 50 MW recompression cycle with dry cooling were shown in Ref. [22], even if, as stated by the authors, the adoption of the selected candidates should be preceded by a targeted investigation on their thermal stability at the maximum operating temperature of 550 °C. Moving to heat sources at higher temperature such as CSP or nuclear plants (from 550 °C to 700 °C), the use of inert and noble gases, as Helium, Xenon, N_2 and others, could improve the cycle efficiency up to 1–2% points, but cannot turn the supercritical cycle into a condensing transcritical cycle, since the critical temperature of these noble gases is lower than the one of the CO_2 [23,24]. On the other hand, inorganic compound such as $TiCl_4$ or N_2O_4 are suitable for blending the CO_2 when high temperature heat sources (above 550 °C) are available leading to thermodynamic efficiencies of the resulting transcritical cycles in the range of 49% with a maximum temperature equal to 700 °C. This efficiency is higher than the corresponding one calculated for pure CO_2 cycles [4,25,26]. Moreover, the reduction in the costs of the power block was shown to be significant, especially if compared to traditional steam Rankine cycles [25].

This work explores the application of another class of compounds, the perfluorocarbons, in the field of the CO_2 blends. Perfluorocarbons are characterised by good solubility into CO_2, good molecular complexity, low-toxicity and low-flammability [27] and they are potentially thermally stable and chemically inert at temperatures higher than 400 °C [26,28–30]. As an example, recent studies investigated the behaviour and the performance of the CO_2 blended with the perfluorohexane C_6F_{14}, showing that the limiting maximum temperature is 450 °C [31]. In this work, the hexafluorobenzene C_6F_6, already proposed in Ref. [32], is selected as its aromaticity makes it the best candidate for achieving higher temperature stability [33]. As a matter of fact, there are no thermal stability data available in the literature for this fluid but just few experimental thermal stability test with both static and dynamic systems revealed that a mixture of pentafluorobenzene C_6HF_5 and hexafluorobenzene (with a composition of 60% and 40% molar fraction respectively) can work at around 480 °C [28]. In order to overcome the lack of information about the fluid behaviour at higher temperatures, new experimental tests on the mixture CO_2 + C_6F_6 are now ongoing within the SCARABEUS project.

The benefits in adopting a mixture as working fluid in a transcritical cycle for CSP application are strictly related to model the mixture thermodynamic behaviour. As a consequence, the components design and the performance of the power cycle is influenced by the prediction of the thermodynamic behaviour of the mixture. Therefore, significant efforts must be devoted to correctly predict the thermodynamic properties of the mixture. Regarding the binary mixture CO_2+C_6F_6, only one data set of experimental bubble points for seven isothermal vapour-liquid equilibrium (VLE) conditions (from 20 to 80 °C) are available in literature for the calibration of thermodynamic properties [34], whereas a reliable property modelmodel should be calibrated and optimized with a significant numbers of experimental data such as VLE, liquid density and speed of sound, in order to reproduce the real mixture behaviour. The aim of this work is to identify the differences in the

Table 1
Examples of compression processes in three different thermodynamic cycles for CSP application with $T_{max} = 550$ °C and $T_{min} = 51$ °C.

	Steam Rankine cycle	Recompressed sCO_2 cycle	Transcritical CO_2+Propane cycle
Compression/Expansion power	~ 3%	~ 34%	~ 15%
Compression ΔT	< 0.01 °C/bar	~ 0.4 °C/bar	~ 0.15 °C/bar

power cycle operating conditions, performance and components design for potentially interesting mixture whose thermodynamic characteristics are not defined, through a variety of Equation of State (EoS), using the available information in open literature and without performing additional experiments. Over the last years, the Peng Robinson (PR) [35] has become the consolidated choice among all the available cubic EoS [36] and it is widely used also for power cycles calculations. Although many different modifications of the first formulation have been developed in the last years, the basic original version of the equation with the classical van der Waals mixing rules is chosen as reference model. Then, a comparison with other typical EoS and property models for supercritical CO_2 cycle is assessed using the software Aspen Plus [37]. Aspen Plus is a commercial software designed for modelling chemical processes and power cycle for several applications. This well-known tool has been already applied to a large variety of plant simulations. Aspen can calculate mass and energy balances as well as several specific component parameters starting from a component library or user-defined components model.

A complete analysis of a CO_2+C_6F_6 transcritical cycle for arid sites with air condenser is carried out in the following sections. The analysis is focused on the maximum cycle temperature $T_{MAX} = 550°C$, with a sensitivity analysis at $T_{MAX} = 700°C$. Starting with Section 2 a literature review of the property model for the modelling of binary mixtures is presented, together with a description of the main drawback of the models based on cubic EoS. In Section 3 the cycle performance is described with PR EoS. In Section 4 the results of the cycle calculations made with various different EoS are discussed and compared. Finally, Section 5 presents the comparison between the different models if the hypothesis of the cycle is altered one at a time.

2. CO_2 mixtures: thermodynamic property evaluation

The accuracy of CO_2-based power cycle modelling is based on the selection of the proper EoS for the evaluation of the thermodynamic properties in all the phase regions. The development and the extension of EoS is still ongoing for several applications, especially in the wide field of binary or multi-component mixtures such as innovative power cycle and chemical processes (e.g. distillation, fluid extraction) [38]. Regarding the pure CO_2, the reference model to calculate its behaviour is the Span-Wagner EoS [39], available in the Reference Fluid Thermodynamic and Transport Properties (REFPROP) developed by the National Institute of Standard and Technology (NIST) [40]. This tool is also able to predict the properties of some CO_2-based binary mixtures, but the database is limited only to common fluids such as hydrocarbons and refrigerants.

For this reason, over the last years, cubic EoS such as PR [35] or Redlich Kwong Soave (RKS) [41] and their variations [36] were proposed for binary mixtures of CO_2 with metal halide or perfluorocarbons [25,31]. Generally, the cubic EoS are versatile models that can give pretty accurate results starting from few parameters of any pure component (critical point, Pitzer acentric factor and molar mass) and can be easily extended to mixtures introducing the most appropriate mixing rules and calibrating the binary interaction parameters (BIP, also named $k_{i,j}$ in cubic EoS) from experimental VLE data [42]. Moreover, the virial model Lee Kesler Plöcker (LK-PLOCK) [43,44] was indicated as a possible candidate for the description of pure CO_2 [45] and recent studies [7] proposed it adding hydrocarbons to pure CO_2 to accurately predict the properties near the critical point of a CO_2-based mixture. In addition, the predictive perturbated chain statistical associating fluid theory (PC-SAFT) model is gaining attention not only for polymeric fluids, since it can be conveniently applied also for non-polymeric, nonpolar, size-asymmetric systems [46]. PC−SAFT can describe phase equilibria for a large variety of including also binary CO_2 mixtures, using a single system dependent interaction parameter [47,48].

2.1. Equations of state validation on known mixtures

All the EoS can compute any thermodynamic property "π" of pure fluids and mixture, with different accuracy, as:

$$\pi(T,P) = \pi_{ideal}(T,P) + \Delta\pi_{residual}(T,P) \tag{1}$$

where the term $\pi_{ideal}(T,P)$ is the property computed in the ideal gas state, while the term $\Delta\pi_{residual}(T,P)$ is the residual property, both evaluated at the same given temperature and pressure. The prediction of real fluid behaviour, thus the residual quantities, strongly affects a power cycle modelling.

If a cubic equation of state is employed, as well as in any other model where the solution of the equation is expressed in the form $v = f(T, P)$, the residual quantities of the main thermodynamic variables such as enthalpy, entropy and specific heat can be calculated as:

$$\Delta h_{residual}(T,P) = \int_0^P \left(v - T\left(\frac{\partial v}{\partial T}\right)_P \right)_T dP \tag{2}$$

$$\Delta s_{residual}(T,P) = \int_0^P \left(\frac{R_g}{P} - \left(\frac{\partial v}{\partial T}\right)_P \right)_T dP \tag{3}$$

$$\Delta C_{P\,residual}(T,P) = -\int_0^P T\left(\left(\frac{\partial^2 v}{\partial T^2}\right)_P \right)_T dP \tag{4}$$

Considering that specific works of CO_2-based mixtures cycle are very low (in the range of 80−120 kJ/kg), the accuracy in enthalpy calculation is fundamental: as a matter of fact, an enthalpy error of 5 kJ/kg in the calculation of any thermodynamic points of the cycle has a relevant impact on the assessment of the cycle efficiency, while this is not true for traditional steam Rankine cycles that are characterised by a specific work of an order of magnitude higher (around a thousand of kJ/kg).

As already mentioned, the equation of state implemented in Refprop for CO_2 (Span and Wagner [39]) can be considered the reference model for pure sCO_2; moreover an equation of state explicit in the Helmholtz free energy as a function of density, temperature, and composition, GERG-2008 [49,50], is adopted in Refprop for a limited number of binary mixtures of CO_2 with some hydrocarbons. In this case, the residual part of the reduced Helmotz free energy of the mixture is a function of the reduced mixture density and the inverse reduced mixture temperature where 4 binary parameters of the reducing functions ($\beta_{v,i,j}$, $\beta_{T,i,j}$, $\gamma_{v,i,j}$, $\gamma_{T,i,j}$) and a binary specific departure function ($F_{i,j}$) can be obtained by fitting experimental data of binary mixtures. As the hexafluorobenzene is not present in the NIST Refprop program, the purpose of this section is to compare the quality of PR EoS with a multi-parameter EoS on CO_2-based mixtures that both softwares (Aspen and Refprop) can simulate. Thus, before moving to the analysis on the investigated mixture CO_2+C_6F_6, a comparison between the cubic EoS and Refprop on known mixtures is briefly discussed, highlighting the benefits and drawbacks related to the adoption of a cubic EoS. In particular, among the many cubic EoS and their variations, the standard PR EoS [35] with the Soave alpha function and van der

Waals mixing rules (with the proper $k_{i,j}$ values fitted on VLE data of each mixture) is selected because it is the standard choice for many cycle simulations. Considering that the ideal gas properties are not affected by the EoS, Fig. 1 presents the residual enthalpy deviation in absolute values computed by PR with respect to the models implemented in Refprop for two CO_2-based mixtures: CO_2+Propane (C_3H_8) and CO_2+Toluene (C_7H_8). As shown in Table 2, the binary parameters of the GERG-2008 reducing functions are fitted to experimental data for both the mixtures, while the additional specific departure function is present just for the CO_2+Toluene mixture.

From Fig. 1, it is possible to notice a significant positive deviation (blue bubbles) of the enthalpy computed by PR in the liquid region for both the mixtures; on the other hand, a slight negative deviation (orange bubbles) can be seen in supercritical conditions. As these two contributions have an opposite sign, the uncertainty on the calculation of enthalpy and, as a consequence, the enthalpy difference between two points in the two different regions (from liquid to supercritical zones) could have a big impact on the evaluation of the cycle efficiency. For example, in a simple recuperative transcritical cycle (layout in Section 3 Fig. 4), an error in the calculation of the enthalpy of the outlet of the pump, which is also the inlet of the recuperator in the high-pressure side, will have an effect on the estimation of recuperated heat, thus on the cycle efficiency.

2.2. Equation of state for sCO$_2$-mixture and binary interaction parameter regression from VLE experimental data

After describing the limiting factors of traditional cubic EoS in cycle calculations, five models are selected in this work for the technical assessment of the power cycle. These models are: (i) simple Peng Robinson EoS with van der Waals mixing rules (PR) [35], (ii) the model that uses the Peng Robinson cubic equation of state with the Boston-Mathias alpha function (PR-BM) [51], (iii) the

Table 2
GERG 2008 EoS: binary parameters and departure functions of CO_2+Propane (C_3H_8) and CO_2+Toluene (C_7H_8).

jth component	$\beta_{T,CO2,j}$	$\beta_{V,CO2,j}$	$\gamma_{T,CO2,j}$	$\gamma_{V,CO2,j}$	$F_{CO2,j}$
C_3H_8	1.0336	0.9969	0.90877	1.0476	0
C_7H_8	1.0	1.047	1.024	1.134	1.257

Table 3
Main characteristics of pure components.

Parameter	units	CO_2	C_6F_6
MW	kg/kmol	44.01	186.06
T_C	°C	31.0	243.3
P_C	bar	73.80	32.75
ω	–	0.2251	0.3989
Z_c	–	0.2735	0.2616

Predictive Soave-Redlich-Kwong (PSRK) equation-of-state model, which is an extension of the RKS equation of state [52], (iv) the virial model LK-PLOCK [43,44] and (v) the PC-SAFT [46]. All the models are available in Aspen Plus and Aspen Properties [37], so this software was used for the thermodynamic property assessment and the modelling of the power cycle assessment. In Annex A (Fig. A.1 and Fig. A.2), a comparison of the calculation of the pure fluids properties (such as liquid density, saturation pressure, liquid specific heat capacity and enthalpy of evaporation) of CO_2 and C_6F_6 using the selected models with respect to the experimental data taken from NIST database [53] is showed.

Table 3 summarizes the main pure component parameters that are required by the different EoS for the definition of the mixture behaviour. The PC-SAFT model needs additional and specific pure components parameters for non-polymer components: (i) the adimensional characteristics segment number *m*, (ii) the adimensional characteristic segment size parameter σ and (iii) the

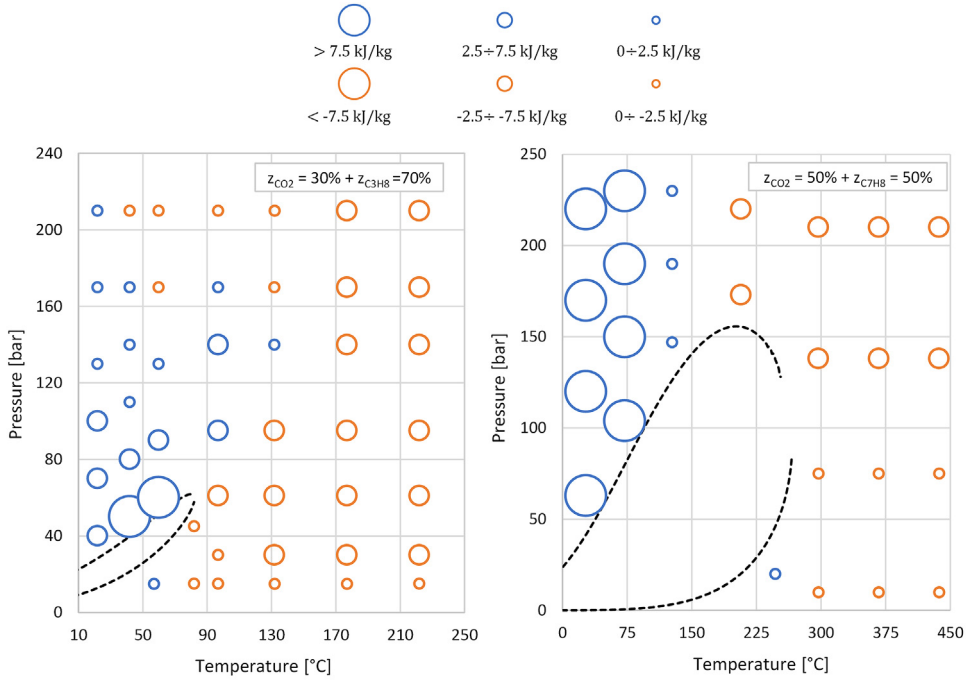

Fig. 1. Differences between residual enthalpy computed with PR with respect to the models implemented in Refprop ($\Delta h_{PR} - \Delta h_{Refprop}$): on the left for the mixture $z_{CO_2} = 30\%$ and $z_{Propane} = 70\%$, on the right for $z_{CO_2} = 50\%$ and $z_{Toluene} = 50\%$. Dashed lines represent the saturation curves modelled by the Refprop models.

Table 4
PC-SAFT parameters of pure components modelled in Aspen Plus.

Parameter	units	CO_2	C_6F_6
m	–	2.569	3.779
ε/k	°C	−121.05	−51.50
σ	–	2.564	3.396

characteristic segment energy parameter ε/k. Table 4 shows these PC-SAFT parameters for the investigated components: the values of pure CO_2 are taken from the Aspen Plus database [37], while the values of C_6F_6 are a results of a regression on the saturated liquid heat capacity at constant pressure ($C_{P,L}$), the density at saturated liquid conditions (ρ_L) and the vapour pressure of pure C_6F_6 as function of the temperature. All these pure C_6F_6 data are taken from NIST database (for a temperature range of 15 °C–230 °C) [53].

The prediction of the mixture thermodynamic properties should consider the interaction between the different fluids that mostly affects the partial molar properties and the partial derivatives of the variables computed for the mixture: for this reason, VLE experimental data can be used to empirically calibrate the BIP of the investigated EoS. In a cubic EoS, the BIP parameter helps on the description of the intermolecular reaction, while the same approach was also used with the PC-SAFT EoS where BIP is introduced to correct the segment-segment interactions of unlike chains [46]. In this work, Aspen Properties [37] is used to determine the coefficients $k_{i,j}$ for the considered mixtures of CO_2 and C_6F_6 starting from experimental VLE data that are available only for the bubble point compositions of seven isotherms, from 20 °C to 80 °C [34]. This optimization on VLE leads to the identification of the minimum pressure of the cycle. Considering that the investigated power cycle does not work on temperature below 50 °C, for the purpose of this work, it has been chosen to optimize the BIP only in the range $50°C - 80°C$ with the least square method.

Table 5 reports the results of the regression procedure for all the four non-predictive investigated thermodynamic models. Being PSRK the only predictive model and given its already satisfactory capability in fitting VLE data for this mixture, no BIP was applied to this model.

The resulting mixture behaviour in P-T plane is reported in Fig. 2 for three different molar compositions and for all the five models, together with the experimental bubble points. It is possible to notice that the two EoS that are based on the same formulation (PR and PR-BM) present very similar results: the different alpha function introduces small deviations just in the region around critical point On the other hand, the virial LK-PLOCK and PC-SAFT EoS are also somehow in agreement. Finally, the PSRK equations produces results between the other models. Although at low temperature all equations converge on the same results, big differences can be noticed at higher temperatures where they diverge, close to the critical point, being this region the most difficult to be modelled.

The saturation lines, presented in Fig. 2, are for high CO_2 molar content because it is the most interesting range for the application of this mixture in thermodynamic cycles. Fig. 3 reports the critical point locus of the mixture, obtained using the PR EoS and its proper BIP. The required characteristics of the mixture for the application in transcritical cycle are mostly related to the critical temperature and molar weight: on the one hand, more C_6F_6 can ensure higher critical temperature (90–100 °C) so to have the whole compression phase in the liquid region, on the other hand a dominant C_6F_6 mixture increases the molar weight of the mixture and would penalize the good characteristics of the CO_2 in supercritical conditions. For these reasons, the analysis can be focused on mixture with CO_2 molar fraction between 70% and 90%.

Table 5
Regressed binary interaction parameters $k_{i,j}$ for the considered mixtures.

EoS	$k_{i,j}$
PR	0.033
PR-BM	0.038
LK-PLOCK	0.080
PC-SAFT	0.040

3. Power cycle design with PR EoS

Among several sCO_2 cycle layouts proposed in literature, a simple recuperative transcritical cycle configuration can be adopted using CO_2-based mixture as working fluid [9]. No multiple pressure levels are strictly required, since the compression is performed in a single pump that can ensure a liquid stream at its outlet, no bleedings are present because the recuperator performs the whole thermal duty exchange, and no reheat are strictly needed. The possibility to use a condensing cycle significantly reduces the advantages of more complex plant layout (i.e. the recompressed cycle) especially if a heavy mixture is employed [25].

The performances of a simple recuperative cycle working with the CO_2+C_6F_6 mixture are investigated in Aspen Plus [37]. As a Rankine cycle, the layout in Fig. 4 (left) considers the pumping of the mixture from saturated liquid conditions (point 1), then the working fluid is preheated in the recuperator (from 2 to 3), reaching the maximum cycle temperature after the primary heat exchanger (point 4). Thus, the mixture is expanded in the turbine (from 4 to 5) and partially cool down in the recuperator (from 5 to 6) before entering the condenser. An example of the T-s (Temperature-Entropy) diagram for a selected mixture is reported in Fig. 4 (right). The main assumption for the cycle performance are presented in Table 6: the minimum temperature is chosen in order to ensure condensation with an air-cooled condenser in hot and arid regions (typical ambient temperature equal to 35 °C [25]). The two maximum temperatures are selected with respect to the assumptions on HTFs characteristics: a base case at 550 °C with the adoption of molten salts; an advanced configuration with liquid sodium reaching a maximum temperature up to 700–750 °C [3,7]. The other parameters of the simple recuperative transcritical cycle, such as pump efficiency and the minimum internal temperature approach, are taken from literature [4]. The maximum pressure of the cycle, at pump outlet, is assumed equal to 250 bar without pressure drop, while it is increased up to 257.5 bar, accounting for the total cycle pressure drop of 7.5 bar distributed in the various cycle components, as reported in Table 6.

Regarding the turbine, a specific numerical tool designed to optimize multistage axial turbines including real gas effects and based on pseudo-1D approach was applied [54]: this model was already adopted for supercritical CO_2 cycles [12]. A rotational speed of $n = 3000\ rpm$ was set for a direct connection of the electric generator to the common electric grid (i.e. frequency of 50 Hz) avoiding the introduction of a gearbox. The low rotational speed coupled with the relatively high mass flow rates implies a significant number of stages, thus the higher the efficiency the higher the turbine dimensions, hence the costs. A preliminary optimum design was selected with seven stages and an efficiency $\eta_{Turbine}$ equal to 91.9%.

The cycle is designed for a gross mechanical power output of 100 MW_{el}. As introduced in the introduction, the first analysis of the cycle design is carried out with the classical Peng Robinson EoS and the corresponding optimized k_{ij}, looking at the optimal mixture composition for achieving the maximum cycle efficiency. Fig. 5

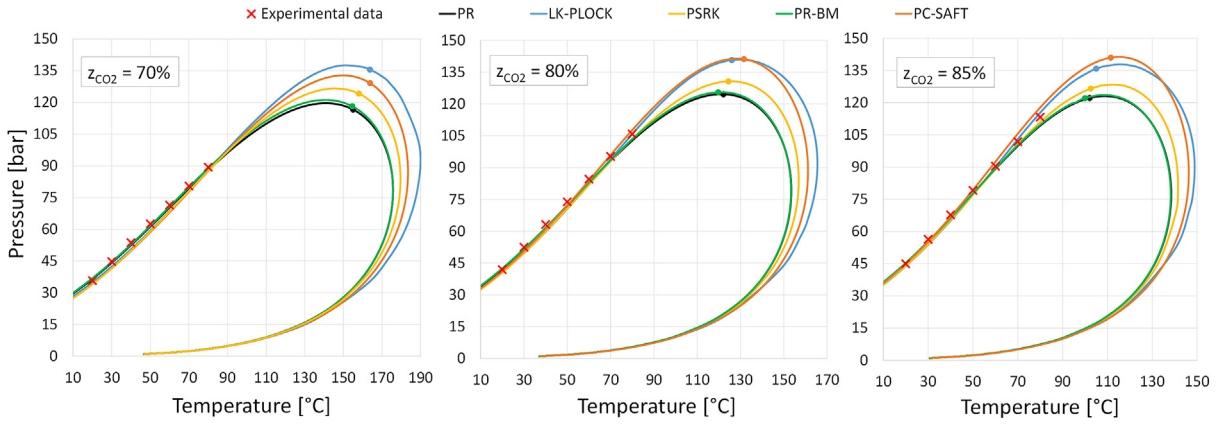

Fig. 2. *CO_2–C_6F_6 mixture: Examples of phase behaviour at different mixture compositions on P-T diagram. Saturation lines calculated with the five investigated models. The reported crosses are experimental data on the bubble line from* Ref. [34].

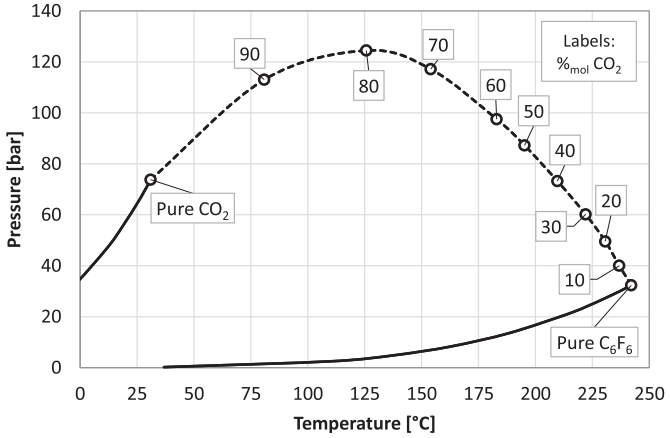

Fig. 3. CO_2–C_6F_6 mixture: Critical point locus on P-T diagram using PR EoS. Labels identify the critical point of the mixture with different CO_2 molar fraction.

shows the resulting cycle efficiency and the recuperator effectiveness, defined in Eq. (6) and Eq. (7), at different mixture molar composition with two investigated maximum cycle temperature. The most efficient composition is identified at $z_{CO2} = 84\%$, with an efficiency of 41.9%: the variation in efficiency is not negligible in the investigated mixture composition range. The same trend can be seen at 700 °C with a maximum efficiency of 47.8%, about 6% points higher than the base case. A possible future development can explore, from an economic perspective, the choice of the mixture composition in this wide range where the efficiency is fairly constant.

Table 6
Assumptions for the power cycle simulations.

Parameters	units	Values[a]
Minimum Temperature (at pump inlet)	°C	51 (41–46)
Vapour fraction at pump inlet	–	0
Maximum Temperature	°C	550/700 (500–600)
Pressure at pump outlet	bar	257.5 (220–280)
ΔT_{MIN} in the Recuperator (MITA)	°C	5 (2.5–7.5)
ΔP_{LOSS}*RecuperatorHP*	bar	0.5 (0–0.5)
ΔP_{LOSS}*Primary Heat Exchanger*	bar	4 (0–4)
ΔP_{LOSS}*RecuperatorLP*	bar	1 (0–1)
ΔP_{LOSS}*Condenser*	bar	2 (0–2)
Turbine Isentropic Efficiency	%	91.9 (90–93)
Pump Isentropic Efficiency	%	88 (82–88)

[a] The range of interest shown between brackets is explored in the sensitivity analysis of section 5.

$$\eta_{Cycle} = \frac{W_{Turbine} - W_{Pump}}{Q_{in}} \tag{6}$$

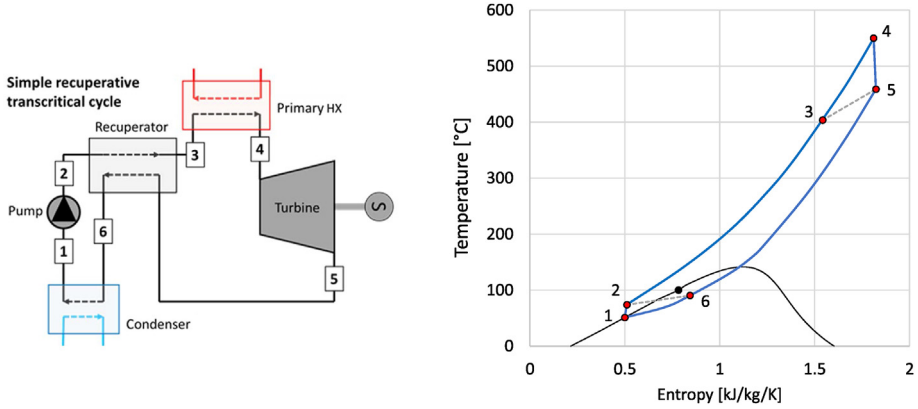

Fig. 4. Plant layout of the cycle working with CO_2 mixtures (left). Example of T-s diagrams of the simple recuperative condensing supercritical cycle for the mixture with at $z_{CO2} = 84\%$ (right). The dashed lines represent the inlet–outlet conditions of the recuperative heat exchanger.

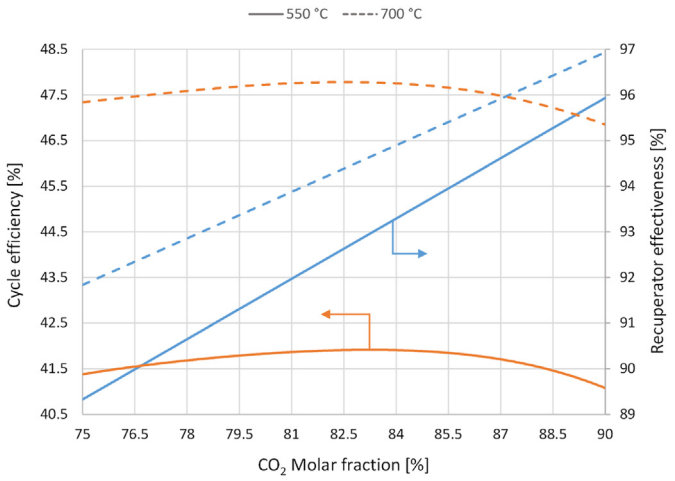

Fig. 5. Cycle efficiency and recuperator effectiveness as a function of the mixture molar composition at two different maximum temperature (Solid lines: $T_{Max} = 550\,^{\circ}C$. Dotted lines: $T_{Max} = 700\,^{\circ}C$).

$$\varepsilon_{Rec} = \frac{Q_{Recuperated}}{Q_{\infty}} = \frac{h(T_3, P_3) - h(T_2, P_2)}{h(T_5, P_5) - h(T_2, P_6)} \quad (7)$$

Some of the most representative results of this sensitivity analysis on the mixture compositions are presented in Table 7 and Table 8 for $T_{MAX} = 550°C$: they are focused on three different CO_2 molar fraction around the maximum efficiency point (80.5%mol, 84%mol, 87.5%mol). Table 7 summarises the thermodynamic properties of all the streams while the power balance and cycle performance are reported in Table 8.

On the high-pressure side of the cycle, significant variations are visible in the temperatures: the higher the CO_2 content in the mixture, the higher the compressibility effects in the pump, and therefore T_2 will increase. On the low-pressure side of the cycle, the temperature levels are closer and the minimum pressure at the inlet of the pump experiences modest variations.

Considering the power balance of the cycle, the higher the CO_2 content the lighter the working fluid, therefore the pump consumptions and turbine productions increase, while the size of the recuperator (both considering the heat exchanged and the UA) is slightly affected. Moreover its effectiveness increases even at constant minimum internal temperature difference (MITA): as a matter of fact, the optimal composition for the cycle efficiency does not correspond to the one which maximizes the recuperator effectiveness. This trend occurs because the higher the CO_2 content, the higher is the heat transferred in the recuperator in the single-phase region, increasing the recuperator effectiveness. This is also confirmed by the Temperature-Heat exchanged (T-Q) diagram of the recuperator for the resulting optimal molar composition in Fig. 6, where the MITA corresponds to the dew point of the mixture in the low-pressure side (at around 78% of exchanged heat). This is a common characteristic of the T-Q diagram of a Printed Circuit Heat Exchangers (PCHE) working with heavy CO_2-mixture: depending on the mixture, the MITA is found either at the dew point of the low-pressure side or inside the VLE region of the low-pressure side. Thanks to the compactness of PCHE, in fact, they are often proposed as an optimal solution for the recuperative heat exchangers of compact cycles.

Table 8
Cycle performance at different mixture composition (base case).

Parameter	units	*80.5 %mol CO_2*	*84 %mol CO_2*	*87.5 %mol CO_2*
$\dot{m}$	[kg/s]	1244.4	1212.5	1180.5
W_{pump}	[MW]	25.2	26.2	27.6
Q_{rec}	[MW]	635.7	625.9	610.8
$Q_{TH,in}$	[MW]	239.0	244.9	253.2
W_{turb}	[MW]	125.2	128.8	133.0
Q_{cond}	[MW]	139.0	142.2	147.8
UA_{rec}	[MW/K]	34.4	34.2	33.4
ε_{rec}	[%]	91.8	93.3	94.8
η_{cycle}	[%]	41.85	41.92	41.64

3.1. Influence of the binary interaction parameter

The influence of the binary interaction parameter regressed for PR EoS is studied through a sensitivity analysis for the base case at 550 °C and $z_{CO2} = 84\%$, in order to understand how the uncertainty on the regressed BIP value can affect the cycle performance. The cycle efficiency as function of the $k_{i,j}$ is shown in Fig. 7 for the optimal composition. The results suggest that a significant variation in the BIP does not imply a significant variation in the cycle performance and its main characteristics. The BIP variation has a limited impact in the two-phase region and mixture behaviour at low pressure with a small shift of the main operating condition: moving the $k_{i,j}$ from 0.016 to 0.05, the minimum pressure of the cycle varies from 76.5 to 78.7 bar, causing a consequent pump outlet temperature variation from 71.7 to 72.1 °C. The recuperator effectiveness increases from 92.8% to 93.8%, as well as the temperature at the inlet of the primary heat exchanger (T_3) rises from 402 to 406 °C. This last effect leads to the reduction of the HTF temperature difference in the primary heat exchanger, increasing the required HTF mass flow rate and, as a consequence, the size of the thermal energy storage of the solar plant.

4. Power cycle assessment with different property model

The software Aspen Plus offers several thermodynamics models. Starting from the preliminary analysis with PR EoS, the influence of the property model selection on the cycle performance is hereby discussed. Initially, the optimal composition for the PR EoS ($z_{CO2} = 84\%$) is fixed and results of the base case ($T_{max} = 550\,^{\circ}C$) with other EoS are compared under the same assumptions of Table 6. Then, the cycle efficiency is computed varying both the composition and the

Table 7
Stream thermodynamic properties at different mixture composition (base case).

Cycle Stations	*80.5 %mol CO_2*			*84 %mol CO_2*			*87.5 %mol CO_2*		
	T [°C]	P [bar]	x_{vap} [−]	T [°C]	P [bar]	x_{vap} [−]	T [°C]	P [bar]	x_{vap} [−]
1	51	73.6	0	51	77.6	0	51	81.7	0
2	69.5	257.5	0	71.9	257.5	0	75.2	257.5	0
3	409.1	257	1	404.2	257	1	397.6	257	1
4	550	253	1	550	253	1	550	253	1
5	459.9	76.6	1	457.8	80.6	1	455.1	84.7	1
6	90.8	75.6	0.63	88.7	79.6	0.69	87.5	83.7	0.77

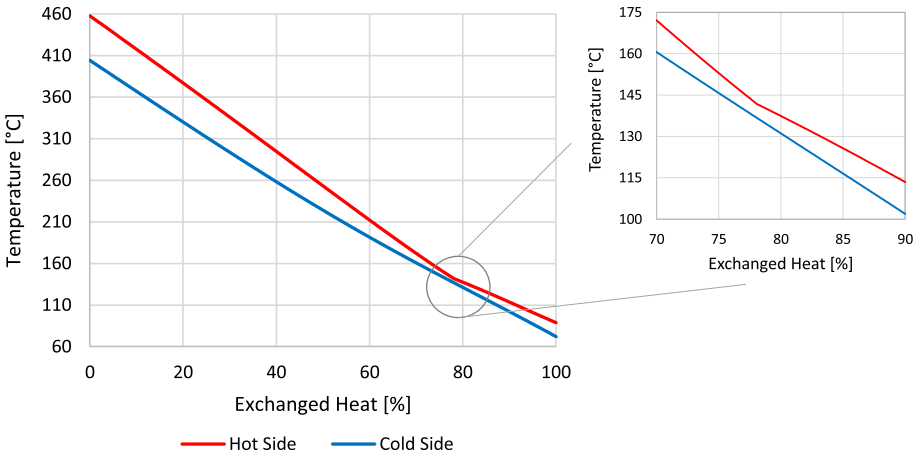

Fig. 6. Temperature-Heat exchanged (T−Q) diagram of the recuperator for mixture with CO_2 molar fraction of 84%mol (base case).

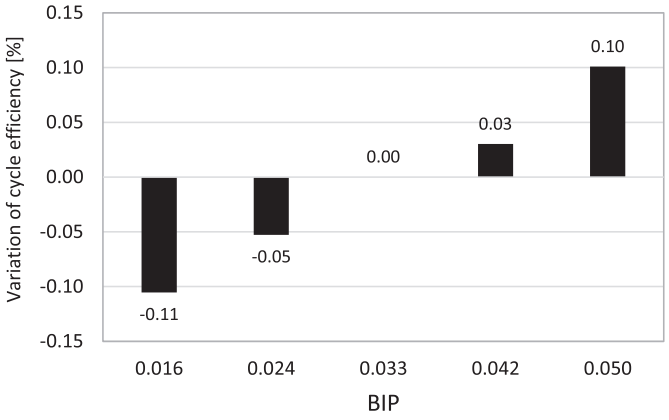

Fig. 7. Influence of BIP on the cycle efficiency for PR EoS (base case).

equation of state.

4.1. Influence of the EoS on the optimized composition with PR EoS

A comparison of the same cycle using different EoS can highlight the inherent uncertainties that the thermodynamic assessment of a cycle brings along. In the following figures, the variation of the heat duties of the heat exchangers involved in the cycle and of the power of the turbomachinery are reported. These can be of interest both for design and for economic perspectives. Furthermore, it is important to investigate whether the most important thermodynamic variable such as the residual enthalpy is constant for every model at some fixed conditions for the cycle (T,P,z), such as pump and turbine inlet. All these effects thus contribute to the cycle design and performance assessment. In Fig. 8, some of the most interesting cycle characteristics are reported using all the five investigated models for the base case ($T_{max} = 550$ °C) considering the mixture composition with a CO_2 molar fraction of 84%.

Starting from the pump, PR and PR-BM are consistent in both the pump power consumption and the temperature increase (T_2-T_1), on the other hand also PC-SAFT and LK-PLOCK reached comparable results, about 7% and 26% lower, respectively, with respect to the cubic EoS, leaving PSRK as an outlier. The important difference in the pump consumption translates into analogous difference in the calculation of T_2, at the pump outlet, that spans in a wide range of $\pm 5°C$, which is a significant deviation if compared to the limited ΔT_{PUMP} of around 20 °C. Considering that the PC-SAFT parameters for the pure fluids are optimized on the saturated liquid properties, as described in section 2.2, this model can be considered more reliable in computing thermodynamic properties in this region.

The residual enthalpy at pump inlet (Residual h_1), that corresponds to a saturated liquid condition, is a good index of the differences between EoS, since it is computed at given (T, P, z) conditions: a significant deviation of about 12 kJ/kg between the two versions of the Peng Robinson EoS and the other three property modelmodels is significant if compared with the limited specific work of the cycle, which is around 80−85 kJ/kg (Fig. 9).

Regarding the estimation of the temperature T_3, the five EoS diverge by up to 6 °C: the variable is computed iteratively by the solver in order to reach convergency on the assumed MITA of the PCHE, and therefore it is a temperature that is significantly affected be the modeling of the heat transferred in the recuperator. For this parameter, even a difference of few Celsius degrees can have a significant impact in the modeling of the receiver of the CSP plant and on the overall performance of the solar power plant.

The residual enthalpy at turbine inlet (Residual h_4), is computed at fixed temperature and pressure, similarly to the Residual h_1, and therefore it can be considered an important variable to underline the differences between the EoS: in this case, PSRK is an outlier, as its numerical value is far from the other model results. This peculiarity of the PSRK model directly translates into an higher turbine production, while, for the other EoS, a more significant Residual h_4 corresponds to a lower turbine specific work. As a matter of fact, excluding PSRK, a difference up to 8 kJ/kg in the calculation of the residual enthalpy at the turbine inlet is unexpected, considering that the mixture behaviour at these operating conditions is close to the ideal gas behaviour.

About the specific heat duties of the recuperator and the condenser, discrepancies up to 10 kJ/kg have an impact on the power block costs. Moreover, especially when an air-cooled condenser is employed, as it is often employed in CSP cycle for arid regions, the auxiliary consumption of the condenser is usually considered proportional to the heat rejected: for this reason, the uncertainties on the heat rejected directly affects also the net power produced by the power plant.

Fig. 9 shows a deviation of the gross specific work, which is defined as $w_{gross} = w_{Turbine} - w_{Pump}$, up to 4 kJ/kg between the models, with respect to an overall value of about 80−85 kJ/kg. A resulting uncertainty of 5% on the specific work directly affects by 5% the cycle mass flow rate, at constant gross power output. This deviation have a big impact on the size of the main cycle

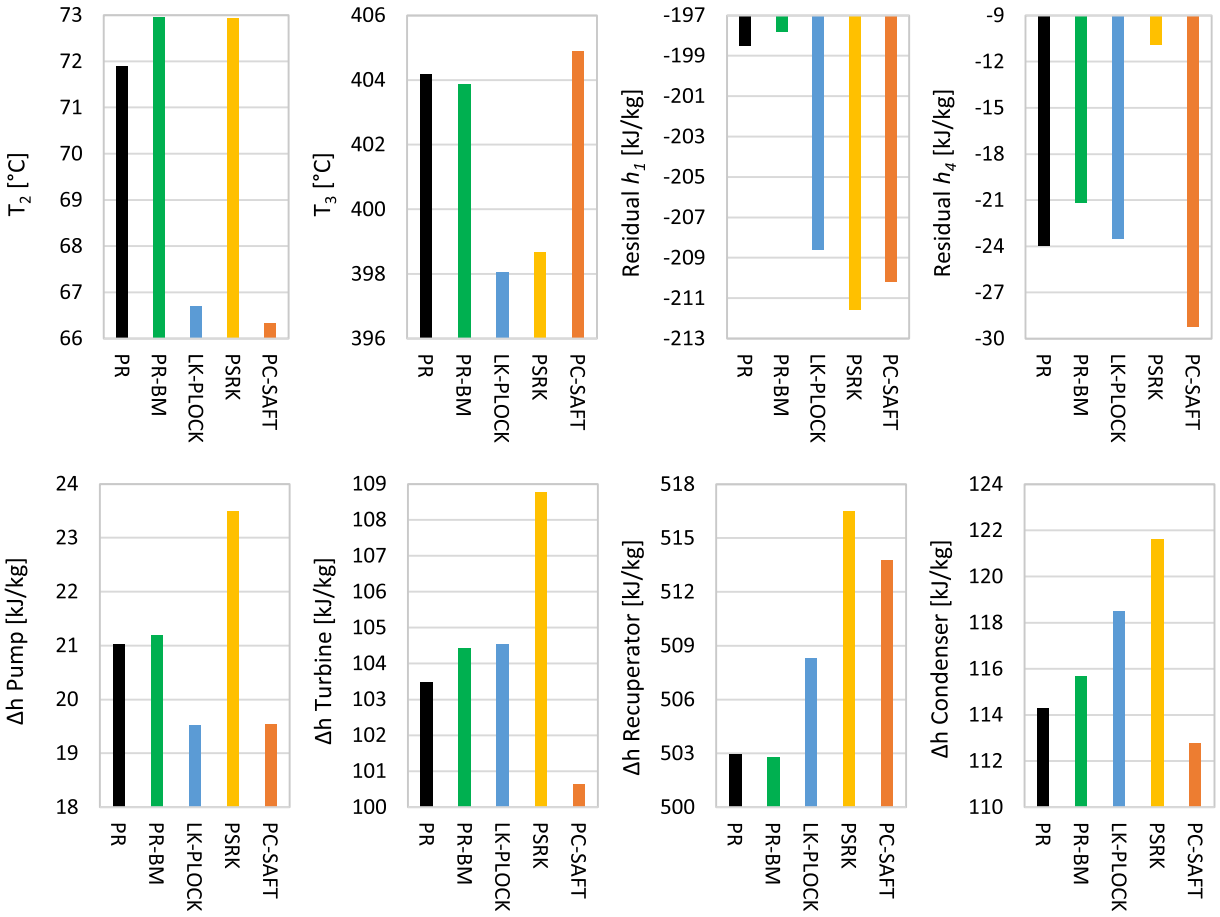

Fig. 8. Comparison of some thermodynamic properties using different property model for a mixture with 84%mol of CO_2 (base case).

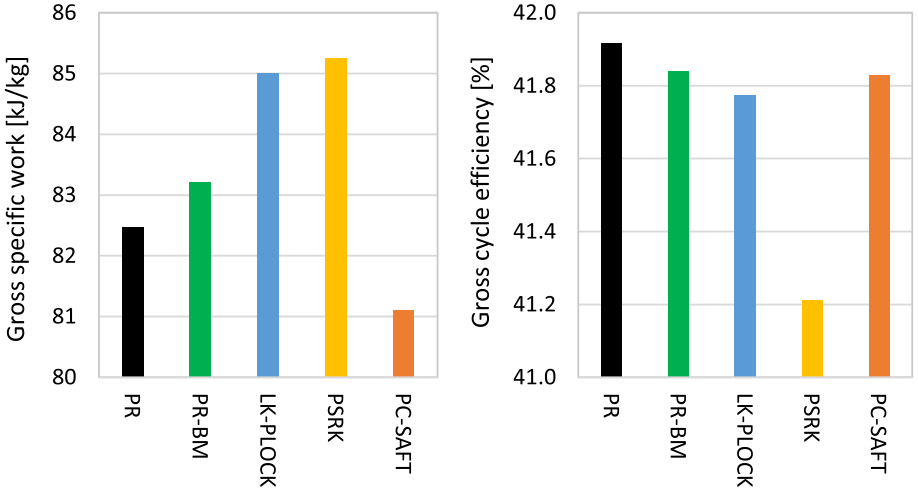

Fig. 9. Cycle performance comparison using different property model for a mixture with 84%mol of CO_2.

components, since they depend both on the specific enthalpy difference and the mass flow rate.

In conclusion, looking at the main parameter for the cycle performance, the gross cycle efficiency, a difference of $\Delta\eta \approx 0.15\%$ can be noticed in Fig. 9, that rises to $\Delta\eta \approx 0.9\%$ taking into account also the PSRK.

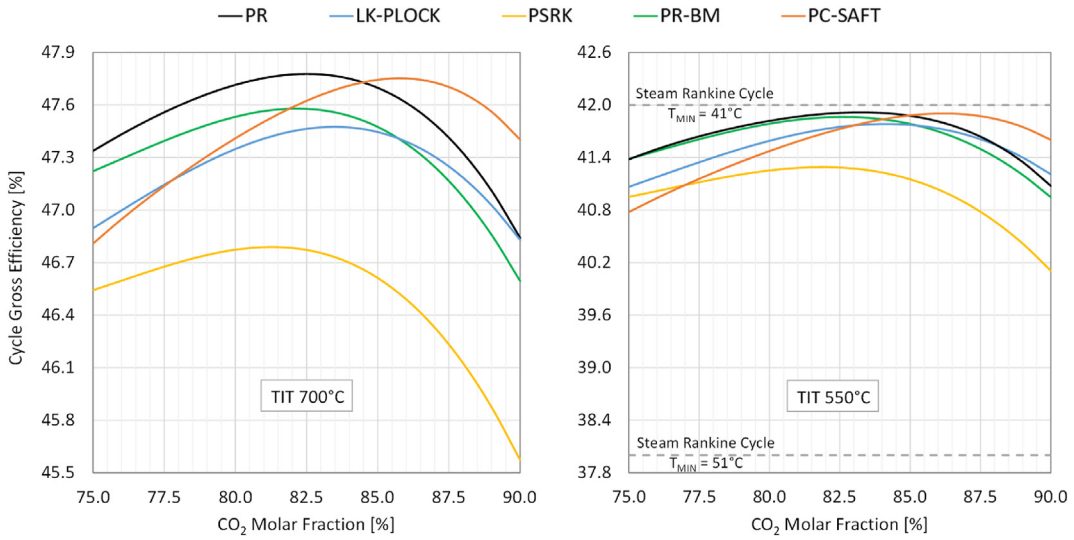

Fig. 10. CO_2+C_6F_6 mixture: cycle gross efficiency as a function of the molar mixture composition using different property models for $T_{Min} = 51°C$ (Left: $T_{Max} = 700$ °C. Right: $T_{Max} = 550$ °C).

Although the difference in cycle efficiency becomes consequential only if medium-large scale power plants are installed, the main outcome of this analysis (the influence of the EoS in the design of the cycle components) is independent from the size of the power plant. This underlines how the choice of the equation of state affects the overall design of the plant, when innovative working fluid are adopted.

4.2. Definition of CO_2–C_6F_6 molar composition for the investigated EoS

A final comparison considering both the mixture composition and the equation of state as degree of freedom is here discussed. This analysis aims at understanding if the definition of the optimum mixture composition is independent from the chosen EoS. The resulting cycle efficiencies are presented in Fig. 10 for a significant range of compositions and for all the five EoS. Both the base case and the configuration with a maximum temperature of 700 °C are represented. Moreover, results are compared with the gross efficiency of a state-of-the art steam-based CSP plant that is characterised by a maximum steam temperature of 550 °C. In Fig. 10 (right), two different reference values are considered, according to different minimum temperatures of the cycle: the upper limit value can be set to 42% with a typical condensing cycle of about 41 °C [5] while the lower limit value of 38% refers to a minimum temperature equal to investigated transcritical cycle (51 °C) [3,4].

The choice of the property model has an influence on two crucial aspect: the cycle performance and the optimum molar fraction. Regarding the base case in Fig. 10 (right), two models, PR-BM and PSRK, identify the optimum mixture composition at $z_{CO2} = 82\%$ with a gross efficiency of 41.8% and 41.3% respectively; the best mixture composition for the LK-PLOCK is aligned with PR results ($z_{CO2} = 84\%$) but with a lower gross efficiency (41.75%). Finally, a maximum efficiency value of 41.9% results at $z_{CO2} = 87\%$ using PC-SAFT model. The performance of the transcritical cycle working with the selected CO_2 blend is always higher than the steam cycle at the same minimum temperature, while a comparison with the steam cycle with a minimum temperature of 41 °C is reported in the sensitivity analysis section.

If the cycle maximum temperature is 700 °C, as shown in Fig. 10 (left), an increase of about 6% points in the cycle efficiency can be noticed with respect to the base case configuration, while keeping a similar trend for each thermodynamic model. In conclusion, All the EoS differ between each other in the identification of both the optimal molar fraction and the actual value of gross cycle efficiency.

5. Sensitivity analysis

A sensitivity analysis was carried out on some appropriate parameters that can substantially vary depending on the power cycle application (i.e. CSP plants, waste heat recovery plants), the environmental conditions (e.g. air ambient temperature) in which the power cycle is installed and also on the economic aspects. Starting from the base case with a mixture molar composition of $z_{CO2} = 84\%$, the objectives of the sensitivity analysis are: (i) to check the influence of the different parameters on the cycle efficiency and (ii) to verify if the cycle efficiency variation is independent from the adopted EoS. The range of interest for each parameter is indicated in Table 6. The analysis is carried out just for the base case configuration with a maximum temperature of 550 °C because no significant influence of the maximum cycle temperature can be shown in relative terms.

Fig. 11 shows the results for all the investigated EoS as an absolute cycle efficiency difference ($\Delta\eta$) with respect to each nominal value found in the previous section: positive variations are on the left side while parameters that cause negative effects are depicted

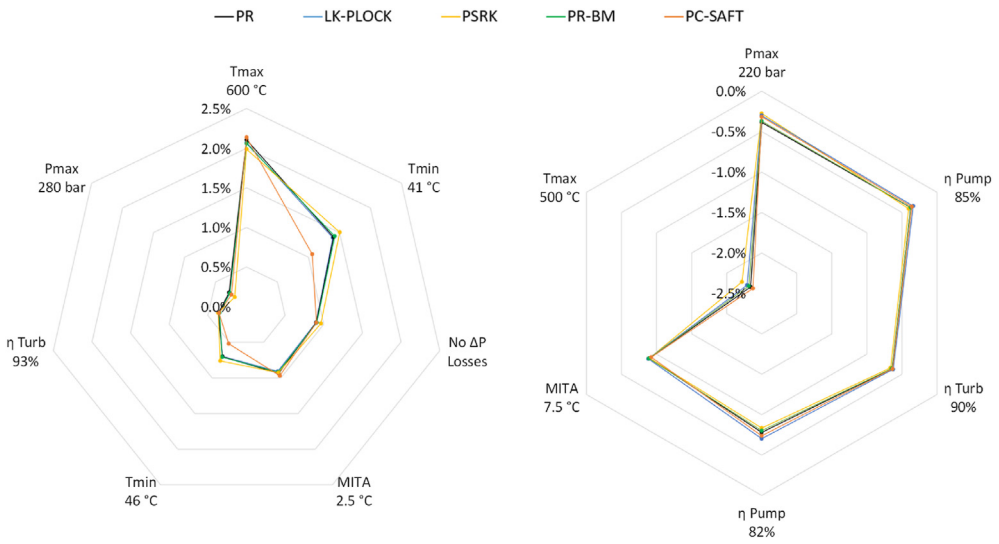

Fig. 11. Variation of cycle gross efficiency through a sensitivity analysis with respect to the reference conditions of the base case defined in Table 6 (Left: positive effect. Right: negative effect).

in the right chart. Fig. 11 outlines the parameters which has the highest impact on the system efficiency. In general, parameters such as maximum temperature and the minimum internal approach have the highest impact on the cycle efficiency with similar results for all the EoS. As expected, the decrease of the minimum temperature together with the increase of the turbomachinery efficiency can have a benefit on the cycle performance. Whereas a small variation of the maximum pressure does not significantly affect the cycle efficiency.

The results confirm that the cycle efficiency variation $\Delta\eta$ is not influenced by the choice of the EoS, with a single outlier: it is represented by the PC-SAFT model when the minimum temperature of the cycle is decreased from its original value of 51 °C, as the modelling of the liquid region is quite different with respect to the other EoS.

In conclusions, the results of Fig. 11 reveal that the transcritical cycle with the mixture CO_2+C_6F_6 at the minimum cycle temperature $T_{MIN} = 41°C$ results, for all the EoS, at least 1% point more efficient than the corresponding steam Rankine cycle at the same minimum temperature.

6. Conclusions

Concentrated solar power plants generally adopt steam cycle to convert thermal energy into electricity. Performance and costs of steam cycle are negatively affected by the limited power output of solar plants and limited maximum temperatures (550 °C) as well as the high ambient temperatures of optimal CSP location. Therefore, R&D activity is focusing on new concepts as sCO_2 cycles to overcome these limitations.

This paper discusses the performance of an innovative working fluid for the exploitation CSP plants: the innovative fluid consists of CO_2 blended with C_6F_6. Since C_6F_6 has a higher critical temperature with respect to CO_2, the blend can be tuned to allow for a condensing cycle even assuming high ambient temperatures (i.e. the mixture can condense up to 70 °C). The calculated gross cycle efficiency of the innovative blend is found to be close to 42% assuming a maximum temperature of 550 °C and adopting a conventional Peng-Robinson Equation of State. Considering that only a limited amount of VLE experimental data are available for this mixture, the selection of the equation of state for the prediction of the mixture behaviour is fundamental, even if it cannot be considered definitive at this stage.

Therefore, the influence of the EoS on the cycle assessments is investigated. Five different EoS were adopted and compared ((i) Peng-Robinson, (ii) Peng Robinson with Boston-Mathias alpha function (iii) the Predictive Soave-Redlich-Kwong (PSRK), (iv) the virial model Lee-Kesler-Plöcker and (v) the PC-SAFT): the results showed a difference in terms of cycle performance which ranged from about 41% to 42% and a variation of the optimal blend composition from a CO_2 molar fraction of 81–87%. Although the maximum efficiency values are quite similar, a detailed analysis on the operating conditions of the cycle components highlighted that components design could be affected by the adopted EoS. For example, variations of about 15% on the pump specific work and of 7% on the turbine specific work is found: these variations can influence the cycle specific work (and therefore its mass flow rate) by up to 5%. Moreover, not negligible percentage deviations are also present in the specific heat duties of the heat exchangers.

Finally, when the maximum temperature is increased to 700 °C the net electric efficiency shifts up to 46.7–47.7% while keeping similar trend for all the EoS.

The next steps will focus on assessing the maximum thermal stability of the CO_2+C_6F_6 mixture to identify the maximum operating temperature and to perform additional Vapour Liquid Equilibrium measurements to improve the calibration of the Equations

of state.

Credit author statement

Gioele Di Marcoberardino: Conceptualization, Methodology, Visualization, Software, Writing – original draft, Review & Editing; Ettore Morosini: Methodology, Visualization, Software, Writing – original draft, Review & Editing; Giampaolo Manzolini: Conceptualization, Project administration, Funding acquisition, Writing – review & editing, Supervision.

Declaration of competing interest

The authors declare that they have no known competing financial interests or personal relationships that could have appeared to influence the work reported in this paper.

Acknowledgements

This paper is part of the SCARABEUS project that has received funding from the European Union's Horizon 2020 research and innovation programme under grant agreement No 814985.

Nomenclature

Acronyms

BIP	Binary interaction parameter,
CSP	Concentrated solar power
EoS	Equation of state
HTF	Heat transfer fluid
LCOE	Levelized cost of electricity, $ MWh^{-1}
LK-Plock	Lee Kesler Plocker EoS
MITA	Minimum Internal Temperature Approach, °C
PR	Peng Robinson EoS
PR-BM	Peng Robinson with Boston-Mathias alpha function EoS
PC-SAFT	Perturbed-Chain Statistical Associating Fluid Theory EoS
PCHE	Printed circuit heat exchanger
PSRK	Predictive SRK EoS
Refprop	Reference Fluid Thermodynamic and Transport Properties
sCO_2	Supercritical CO_2 cycle
VLE	Vapour-Liquid Equilibrium

Symbols

C_P	Heat capacity at constant pressure, kJ kg^{-1} K^{-1}
$\Delta\eta$	Gross cycle efficiency difference,
ΔT	Temperature difference, °C
ΔP	Pressure drop, bar
$\Delta\pi_{residual}$	Residual quantity of the thermodynamic variable π
$F_{i,j}$	Departure function for GERG-2008 EoS
h	Enthalpy, kJ/kg
$k_{i,j}$	Cubic EoS binary interaction parameter,
m	Adimensional characteristic segment number of the component, for PC SAFT EoS,
$\dot{m}$	Mass flow rate, kg s^{-1}
MM	Molar mass, $kgkmol^{-1}$
P	Pressure, bar
Q_{th}	Thermal heat, MW
ρ	Density, kg m^{-3}
s	Entropy, kJ kg^{-1} K^{-1}
T	Temperature, °C
x_i	Species i molar fraction in liquid phase,
y_i	Species i molar fraction in gas phase,
W	Mechanical work, MW
Z	Compressibility factor,
z_i	Molar fraction of the component i

Greek symbols

η_{cycle}	Cycle efficiency,
$\eta_{Turbine}$	Turbine isentropic efficiency,
η_{Pump}	Pump isentropic efficiency,
ε/k	Characteristic segment energy parameter, for PC SAFT EoS, K
α	Vapour quality of the mixture in VLE conditions,
β_T	Binary parameter of the temperature reducing function for GERG-2008 EoS
β_V	Binary parameter of the density reducing function for GERG-2008 EoS
γ_T	Binary parameter of the temperature reducing function for GERG-2008 EoS
γ_V	Binary parameter of the density reducing function for GERG-2008 EoS
σ	Adimensional characteristic segment size parameter, for PC SAFT EoS,
ε_{Rec}	Recuperator effectiveness,
ω	Pitzer acentric factor,

Subscripts

c	Critical
cond	Condenser
i,j	Species
L	Liquid phase
LOSS	Loss
min	Minimum
max	Maximum
pump	Pump
tur	Turbine
vap	Vapour phase

Annex A

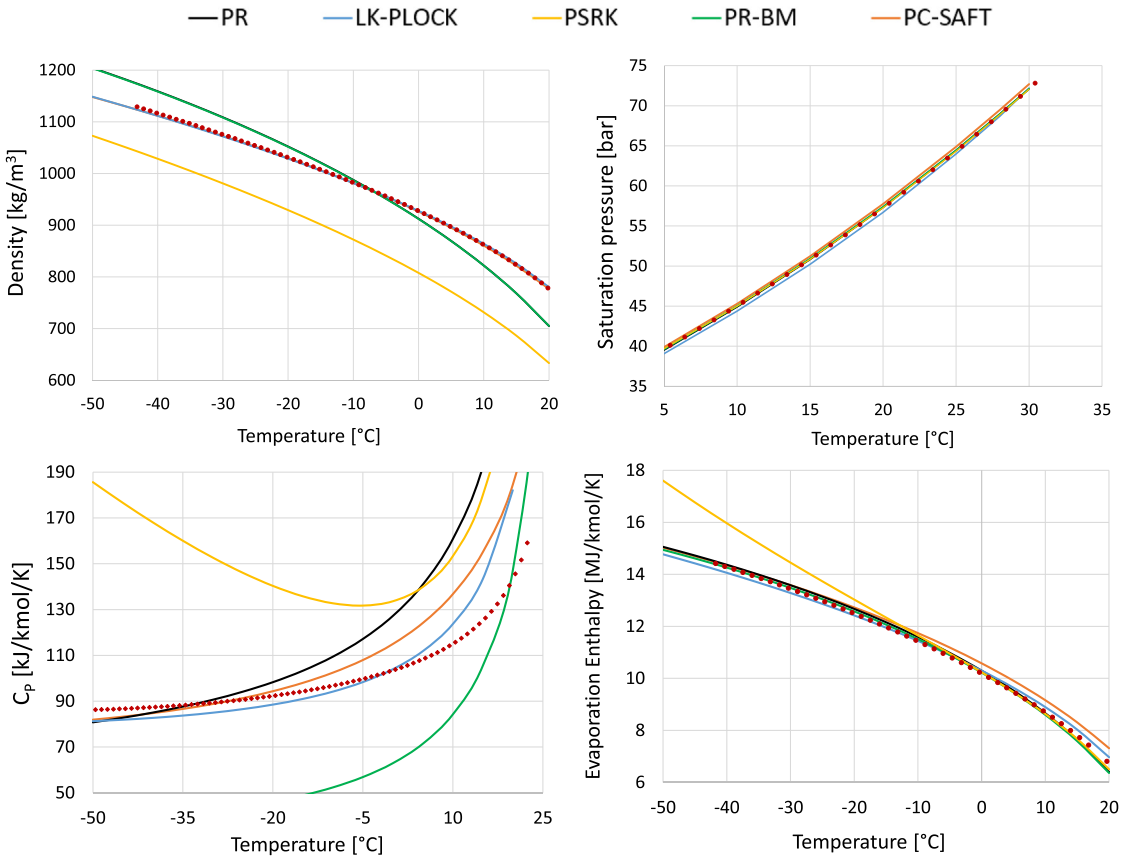

Fig. A.1. *CO_2 pure fluid properties (liquid density, saturation pressure, liquid specific heat capacity, enthalpy of evaporation): comparison of data simulated with the five EoS (solid lines) with respect to the experimental data (dots) taken from NIST database* [53].

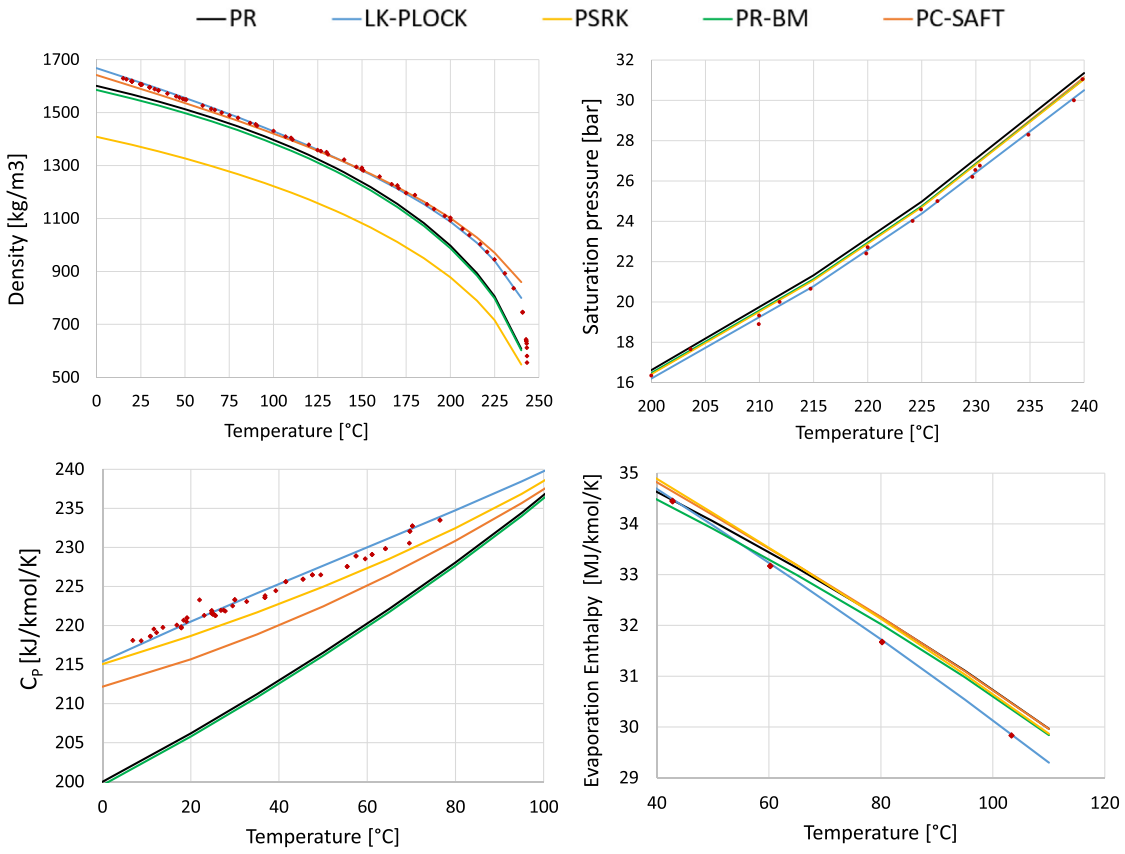

Fig. A.2. *C_6F_6 pure fluid properties (liquid density, saturation pressure, liquid specific heat capacity, enthalpy of evaporation): comparison of data simulated with the five EoS (solid lines) with respect to the experimental data (dots) taken from NIST database* [53].

References

[1] Gauché P, Rudman J, Mabaso M, Landman WA, von Backström TW, Brent AC. System value and progress of CSP. Sol Energy 2017;152:106–39. https://doi.org/10.1016/j.solener.2017.03.072.

[2] Taylor M, Ralon P, Anuta H, Al-Zoghoul S. Renewable power generation costs in 2019. https://www.irena.org/-/media/Files/IRENA/Agency/Publication/2018/Jan/IRENA_2017_Power_Costs_2018.pdf; 2020.

[3] Polimeni S, Binotti M, Moretti L, Manzolini G. Comparison of sodium and KCl-MgCl2 as heat transfer fluids in CSP solar tower with sCO2 power cycles. Sol Energy 2018;162:510–24. https://doi.org/10.1016/j.solener.2018.01.046.

[4] Binotti M, Invernizzi CM, Iora P, Manzolini G. Dinitrogen tetroxide and carbon dioxide mixtures as working fluids in solar tower plants. Sol Energy 2019;181:203–13. https://doi.org/10.1016/j.solener.2019.01.079.

[5] Kelly B, Izygon M, Vant-Hull L. Advanced thermal energy storage for central receivers with supercritical coolants. SolarPaces Conf 2010. https://doi.org/10.2172/981926.

[6] Dudda B, Shin D. Effect of nanoparticle dispersion on specific heat capacity of a binary nitrate salt eutectic for concentrated solar power applications. Int J Therm Sci 2013;69:37–42. https://doi.org/10.1016/j.ijthermalsci.2013.02.003.

[7] Ho CK, Carlson M, Garg P, Kumar P. Technoeconomic analysis of alternative solarized s-CO2 brayton cycle configurations. J Sol Energy Eng 2016;138. https://doi.org/10.1115/1.4033573.

[8] Dunham MT, Iverson BD. High-efficiency thermodynamic power cycles for concentrated solar power systems. Renew Sustain Energy Rev 2014;30:758–70. https://doi.org/10.1016/j.rser.2013.11.010.

[9] Crespi F, Sánchez D, Rodríguez JM, Gavagnin G. A thermo-economic methodology to select sCO2 power cycles for CSP applications. Renew Energy 2020;147:2905–12. https://doi.org/10.1016/j.renene.2018.08.023.

[10] Crespi F, Sánchez D, Sánchez T, Martínez GS, David S, Mart GS. Capital cost assessment of concentrated solar power plants based on supercritical carbon dioxide power cycles. J Eng Gas Turbines Power 2019;141. https://doi.org/10.1115/1.4042304.

[11] Atif M, Al-Sulaiman FA. Energy and exergy analyses of solar tower power plant driven supercritical carbon dioxide recompression cycles for six different locations. Renew Sustain Energy Rev 2017;68:153–67. https://doi.org/10.1016/j.rser.2016.09.122.

[12] Binotti M, Astolfi M, Campanari S, Manzolini G, Silva P. Preliminary assessment of sCO2 cycles for power generation in CSP solar tower plants. Appl Energy 2017;204:1007–17. https://doi.org/10.1016/j.apenergy.2017.05.121.

[13] Lin W, Liangming P, Junfeng W, Deqi C, Yanping H, Lian H. Investigation on the temperature sensitivity of the S-CO2 Brayton cycle efficiency. Energy; 2019. https://doi.org/10.1016/j.energy.2019.04.100.

[14] Saravi SS, Tassou SA. An investigation into sCO2 compressor performance prediction in the supercritical region for power systems. Energy procedia. Elsevier Ltd; 2019. p. 403–11. https://doi.org/10.1016/j.egypro.2019.02.098.

[15] SCARABEUS. Supercritical carbon dioxide/alternative fluids blends for efficiency upgrade of solar power plants. https://www.scarabeusproject.eu/; 2019.

[16] Invernizzi C. Prospects of mixtures as working fluids in real-gas brayton cycles. Energies 2017;10:1649. https://doi.org/10.3390/en10101649.

[17] Invernizzi CM, Van Der Stelt T. Supercritical and real gas Brayton cycles operating with mixtures of carbon dioxide and hydrocarbons. Proc Inst Mech Eng Part A J Power Energy 2012;226:682–93. https://doi.org/10.1177/0957650912444689.

[18] Conboy TM, Wright SA, Ames DE, Lewis TG. CO2-Based mixtures as working fluids for geothermal turbines, albuquerque, vol. 945. California: New Mexico 87185 and Livermore; 2012.

[19] Ayub A, Invernizzi CM, Di Marcoberardino G, Iora P, Manzolini G. Carbon dioxide mixtures as working fluid for high-temperature heat recovery: a thermodynamic comparison with transcritical organic rankine cycles. Energies 2020;13:4014. https://doi.org/10.3390/en13154014.

[20] Sánchez CJN, da Silva AK. Technical and environmental analysis of transcritical Rankine cycles operating with numerous CO2 mixtures. Energy 2018;142:180–90. https://doi.org/10.1016/j.energy.2017.09.120.

[21] Shu G, Yu Z, Tian H, Liu P, Xu Z. Potential of the transcritical Rankine cycle using CO2-based binary zeotropic mixtures for engine's waste heat recovery. Energy Convers Manag 2018;174:668–85. https://doi.org/10.1016/j.enconman.2018.08.069.

[22] Liu X, Xu Z, Xie Y, Yang H. CO2-based mixture working fluids used for the dry-cooling supercritical Brayton cycle: thermodynamic evaluation. Appl Therm Eng 2019;162:114226. https://doi.org/10.1016/j.applthermaleng.2019.114226.

[23] Guo JQ, Li MJ, Xu JL, Yan JJ, Wang K. Thermodynamic performance analysis of different supercritical Brayton cycles using CO2-based binary mixtures in the molten salt solar power tower systems. Energy 2019;173:785–98. https://doi.org/10.1016/j.energy.2019.02.008.
[24] Jeong WS, Lee JI, Jeong YH. Potential improvements of supercritical recompression CO2Brayton cycle by mixing other gases for power conversion system of a SFR. Nucl Eng Des 2011;241:2128–37. https://doi.org/10.1016/j.nucengdes.2011.03.043.
[25] Manzolini G, Binotti M, Bonalumi D, Invernizzi C, Iora P. CO2 mixtures as innovative working fluid in power cycles applied to solar plants. Techno-economic assessment, Sol Energy 2019;181:530–44. https://doi.org/10.1016/J.SOLENER.2019.01.015.
[26] Lasala S, Bonalumi D, Macchi E, Privat R, Jaubert JN. The design of CO2-based working fluids for high-temperature heat source power cycles. Energy Procedia 2017;129:947–54. https://doi.org/10.1016/j.egypro.2017.09.125.
[27] Colina CM, Galindo A, Blas FJ, Gubbins KE. Phase behavior of carbon dioxide mixtures with n-alkanes and n-perfluoroalkanes. In: Fluid phase equilib.; 2004. p. 77–85. https://doi.org/10.1016/j.fluid.2004.06.021.
[28] Dinanno LR, Dibella FA, Koplow MD. An RC-1 organic Rankine bottoming cycle for an adiabatic diesel engine. 1983.
[29] Lasala S, Invernizzi C, Iora P, Chiesa P, Macchi E. Thermal stability analysis of perfluorohexane. In: Energy procedia. Elsevier Ltd; 2015. p. 1575–82. https://doi.org/10.1016/j.egypro.2015.07.358.
[30] Lemal DM. Perspective on fluorocarbon chemistry. J Org Chem 2004;69:1–11. https://doi.org/10.1021/jo0302556.
[31] Di Marcoberardino G, Invernizzi CM, Iora P, Ayub A, Di Bona D, Chiesa P, Binotti M, Manzolini G. Experimental and analytical procedure for the characterization of innovative working fluids for power plants applications. Appl Therm Eng 2020;178:115513. https://doi.org/10.1016/j.applthermaleng.2020.115513.
[32] Lasala EMS, Chiesa P. Binary mixtures of carbon dioxide and fluorocarbons as working fluids for power production applications. In: Conf. Proc. JEEP2014 – 40ième journées d'Etudes des equilibres entre phases; 2014. Lyon, France.
[33] Antonucci JM, Wall LA. High-temperature reactions of hexafluorobenzene. J Res Notional Bur Stand - A Phys Chem 1966;70:473–80.
[34] Dias AMA, Daridon JL, Pa JC. Vapor - liquid equilibrium of carbon dioxide - perfluoroalkane Mixtures : experimental data and SAFT modeling. Ind Eng Chem Res 2006;45:2341–50.
[35] Peng DY, Robinson DB. New two-constant equation of state. Ind Eng Chem Fundam 1976;15:59–64.
[36] Lopez-Echeverry JS, Reif-Acherman S, Araujo-Lopez E. Peng-Robinson equation of state: 40 years through cubics. Fluid Phase Equil 2017;447:39–71. https://doi.org/10.1016/j.fluid.2017.05.007.
[37] AspenTech. Aspen Plus (n.d.), http://www.aspentech.com/products/aspen-plus.aspx.
[38] Wilhelmsen Ø, Aasen A, Skaugen G, Aursand P, Austegard A, Aursand E, Gjennestad MA, Lund H, Linga G, Hammer M. Thermodynamic modeling with equations of state: present challenges with established methods. Ind Eng Chem Res 2017;56:3503–15. https://doi.org/10.1021/acs.iecr.7b00317.
[39] Span R, Wagner W. A new equation of state for carbon dioxide covering the fluid region from the triple-point temperature to 1100 K at pressures up to 800 MPa. J Phys Chem Ref Data 1996;25:1509–96. https://doi.org/10.1063/1.555991.
[40] NIST - National Institute of Standards and Technology. REFPROP - reference fluid thermodynamic and Transport properties (n.d.), https://www.nist.gov/srd/refprop.
[41] Soave G. Equilibrium constants from a modified Redlich-Kwong equation of state. Chem Eng Sci 1972;27:1197–203. https://doi.org/10.1016/0009-2509(72)80096-4.
[42] Sandler SI. Chemical, biochemical, and engineering thermodynamics. fifth ed. 2017.
[43] Lee BI, Kesler MG. A generalized thermodynamic correlation based on three-parameter corresponding states. AIChE J 1975;21:510–27. https://doi.org/10.1002/aic.690210313.
[44] Plöcker U, Knapp H, Prausnitz J. Calculation of high-pressure vapor-liquid equilibria from a corresponding-states correlation with emphasis on asymmetric mixtures. Ind Eng Chem Process Des Dev 1978;17:324–32. https://doi.org/10.1021/i260067a020.
[45] White CW, Weiland NT. Evaluation of property methods for modeling direct-supercritical CO2 power cycles. J Eng Gas Turbines Power 2018;140. https://doi.org/10.1115/1.4037665.
[46] Gross J, Sadowski G. Perturbed-chain SAFT: an equation of state based on a perturbation theory for chain molecules. Ind Eng Chem Res 2001;40:1244–60. https://doi.org/10.1021/ie0003887.
[47] Kontogeorgis GM, Folas GK. Thermodynamic models for industrial applications: from classical and advanced mixing rules to association theories. John Wiley & Sons; 2010. https://doi.org/10.1002/9780470747537.
[48] Werth S, Kohns M, Langenbach K, Heilig M, Horsch M, Hasse H. Interfacial and bulk properties of vapor-liquid equilibria in the system toluene + hydrogen chloride + carbon dioxide by molecular simulation and density gradient theory + PC-SAFT. Fluid Phase Equil 2016;427. https://doi.org/10.1016/j.fluid.2016.07.016.
[49] Kunz O, Wagner W. The GERG-2008 wide-range equation of state for natural gases and other mixtures: an expansion of GERG-2004. J Chem Eng Data 2012;57:3032–91. https://doi.org/10.1021/je300655b.
[50] Kunz O, Klimeck R, Wagner W, Jaeschke M. The GERG-2004 wide-range equation of state for natural gases and other mixtures. http://scholar.google.com/scholar?hl=en&btnG=Search&q=intitle:The+GERG-2004+Wide-Range+Equation+of+State+for+Natural+Gases+and+Other+Mixtures#0; 2007.
[51] Boston JF, Mathias PM. Phase equilibria in a third-generation process simulator. In: 2nd int. Conf. Phase equlibria fluid prop. Chem. Ind.; 1980. Berlin, Germany.
[52] Holderbaum T, Gmehling J. PSRK: a group contribution equation of state based on UNIFAC. Fluid Phase Equil 1991;70:251–65. https://doi.org/10.1016/0378-3812(91)85038-V.
[53] NIST - National Institute of Standards and Technology. NIST ThermoData engine (n.d.), https://www.nist.gov/mml/acmd/trc/thermodata-engine.
[54] Macchi E, Perdichizzi A. Efficiency prediction for axial-flow turbines operating with nonconventional fluids. J Eng Gas Turbines Power 1981;103:718–24.